

V. SUMMARY AND CONCLUSION

In this paper, we have presented a fairly straightforward method for incorporating TS into the estimate of epicardial potentials. Our algorithm incorporates a different spatial smoothing parameter at each time step in the sequence. The total spatial smoothing term is then simply partitioned between temporal and spatial smoothing. In our experiments, we found the weighting of $\beta = 0.25$, corresponding to weighting the spatial smoothing only one third that of the TS, worked consistently well, and the algorithm appeared to be quite robust with regard to the value of this parameter. In examining the match between estimated and measured electrograms, or the match between estimated isopotential maps and measured isopotential maps, the estimates constructed using the new TS algorithm produced consistently smaller relative errors than estimates constructed using the QS algorithm or estimates constructed by postprocessing with a MA filter.

REFERENCES

- [1] P. Colli-Franzone, L. Guerri, S. Tentoni, C. Viganotti, S. Baruffi, S. Spaggiari, and B. Taccardi, "A mathematical procedure for solving the inverse potential problem of electrocardiography. Analysis of the time-space accuracy from *in vitro* experimental data," *Math. Biosci.*, vol. 77, pp. 353–396, 1985.
- [2] P. R. Johnston and D. Kilpatrick, "The inverse problem of electrocardiography: The performance of inversion techniques as a function of patient anatomy," *Math. Biosci.*, vol. 126, pp. 126–145, 1995.
- [3] P. R. Johnston, "The potential for Laplacian maps to solve the inverse problem of electrocardiography," *IEEE Trans. Biomed. Eng.*, vol. 43, pp. 384–393, Apr. 1996.
- [4] P. R. Johnston and R. Gulrajani, "A new method for regularization parameter determination in the inverse problem of electrocardiography," *IEEE Transactions on Biomedical Engineering*, vol. 44, pp. 19–39, 1997.
- [5] B. He, "Principle and applications of the Laplacian electrocardiogram," *IEEE Eng. Med. Biol. Mag.*, pp. 133–138, 1997.
- [6] B. He and D. Wu, "A bioelectric inverse imaging technique based on surface Laplacians," *IEEE Trans. Biomed. Eng.*, vol. 44, pp. 529–538, July 1997.
- [7] Y. Rudy and B. J. Messinger-Rapport, "The inverse problem in electrocardiography: Solutions in terms of epicardial potentials," *CRC Crit. Rev. Biomed. Eng.*, vol. 16, pp. 215–268, 1988.
- [8] B. J. Messinger-Rapport and Y. Rudy, "Noninvasive recovery of epicardial potentials in a realistic heart-torso-geometry," *Circ. Res.*, vol. 66, pp. 1023–1039, 1990.
- [9] H. Oster, B. Taccardi, R. Lux, P. Ershler, and Y. Rudy, "Noninvasive electrocardiographic imaging: Reconstruction of epicardial potentials, electrograms, and isochrones and localization of single and multiple electrocardiographic events," *Circulation*, vol. 96, pp. 1012–1024, 1997.
- [10] R. D. Throne, L. G. Olson, T. J. Hrabik, and J. R. Windle, "Generalized eigensystem techniques for the inverse problem of electrocardiography applied to a realistic heart-torso geometry," *IEEE Trans. Biomed. Eng.*, vol. 44, pp. 447–454, June 1997.
- [11] R. D. Throne, L. G. Olson, and T. J. Hrabik, "A comparison of higher-order generalized eigensystem techniques and Tikhonov regularization for the inverse problem of electrocardiography," *Inv. Prob. Eng.*, vol. 7, pp. 143–193, 1999.
- [12] R. D. Throne and L. G. Olson, "Fusion of body surface potential and body surface Laplacian signals for electrocardiographic imaging," *IEEE Trans. Biomed. Eng.*, pp. 452–462, Apr. 2000.
- [13] H. Oster and Y. Rudy, "Use of temporal information in the regularization of the inverse problem of electrocardiography," *IEEE Trans. Biomed. Eng.*, vol. 39, pp. 65–75, Jan. 1992.
- [14] D. H. Brooks, G. M. Maratos, G. Ahmad, and R. S. MacLeod, "The augmented inverse problem of electrocardiography: Combined time and space regularization," in *Proc. IEEE Engineering in Medicine and Biology Conf.*, vol. 15, 1993, pp. 773–774.
- [15] G. F. Ahmad, D. H. Brooks, C. A. Jacobson, and R. S. MacLeod, "Constraint evaluation in inverse electrocardiography using convex optimization," in *Proc. IEEE Engineering in Medicine and Biology Conf.*, 1995, pp. 209–210.
- [16] D. H. Brooks, K. Srinidhi, D. R. Kaeli, and R. S. MacLeod, "Parallelized convex optimization for joint time/space inverse electrocardiography," in *Proc. IEEE Engineering in Medicine and Biology Conf.*, vol. 4, 1997, pp. 1439–1440.
- [17] D. H. Brooks, G. F. Ahmad, R. S. MacLeod, and G. M. Maratos, "Inverse electrocardiography by simultaneous imposition of multiple constraints," *IEEE Trans. Biomed. Eng.*, vol. 46, pp. 3–18, Jan. 1999.
- [18] G. F. Ahmad, D. H. Brooks, and R. S. MacLeod, "An admissible set approach to inverse electrocardiography," *Ann. Biomed. Eng.*, pp. 278–292, 1998.
- [19] F. Greensite and G. Huiskamp, "An improved method for estimating epicardial potentials from the body surface," *IEEE Trans. Biomed. Eng.*, vol. 45, pp. 98–104, Jan. 1997.
- [20] R. N. Klepfer, C. R. Johnson, and R. S. MacLeod, "The effects of inhomogeneities and anisotropies on electrocardiographic fields," *IEEE Trans. Biomed. Eng.*, pp. 706–719, Aug. 1997.
- [21] R. D. Throne, L. G. Olson, and J. R. Windle, "Improved parameter choice methods and temporal filtering for the generalized eigensystem method applied to the inverse problem of electrocardiography," *Inv. Prob. Eng.*, pp. 339–365, 2001.

A New Real-Time Retinal Tracking System for Image-Guided Laser Treatment

Nahed H. Solouma, Abou-Bakr M. Youssef, Yehia A. Badr, and Yasser M. Kadah*

Abstract—A new system is proposed for tracking sensitive areas in the retina for computer-assisted laser treatment of choroidal neovascularization (CNV). The system consists of a fundus camera using red-free illumination mode interfaced to a computer that allows real-time capturing of video input. The first image acquired is used as the reference image and utilized by the treatment physician for treatment planning. A grid of seed contours over the whole image is initiated and allowed to deform by splitting and/or merging according to preset criteria until the whole vessel tree is demarcated. Then, the image is filtered using a one-dimensional Gaussian filter in two perpendicular directions to extract the core areas of such vessels. Faster segmentation can be obtained for subsequent images by automatic registration to compensate for eye movement and saccades. An efficient registration technique is developed whereby some landmarks are detected in the reference frame then tracked in the subsequent frames. Using the relation between these two sets of corresponding points, an optimal transformation can be obtained. The implementation details of proposed strategy are presented and the obtained results indicate that it is suitable for real-time location determination and tracking of treatment positions.

Index Terms—Contour detection, feature extraction, image registration, retinal tracking.

I. INTRODUCTION

Diabetic retinopathy resulting from long-term diabetes mellitus is one of the common diseases that lead to choroidal neovascularization (CNV). CNV is considered among the most important blinding conditions today. It decreases the amount of blood supplying the retina

Manuscript received September 14, 2001; revised April 17, 2002. This work was supported in part by International Biomedical Engineering (IBE Technologies), Giza, Egypt. *Asterisk indicates corresponding author.*

N. H. Solouma, A.-B. M. Youssef, and Y. A. Badr are with the Biomedical Engineering Department and, Department of Laser Applications in Medicine and Biology, Laser Institute, Cairo University, 12613 Giza, Egypt.

Y. M. Kadah is with the Biomedical Engineering Department, Cairo University, 12613 Giza, Egypt (e-mail: ymk@ieee.org).

Publisher Item Identifier 10.1109/TBME.2002.802059.

especially within the central area of acute vision [1]. Among the currently available treatment strategies is the use of lasers. This method works by aiming an appropriate amount of laser energy to the affected areas of the retina in order to photocoagulate these areas. To obtain satisfactory results, the physician must identify the full extent of CNV and cauterize it completely in order to save the central vision [1], [2]. Several thousands of laser shots are required and care must be taken to avoid radiating the macula (the area of acute vision), optic disc, the blood vessel tree, and the region between the macula and the optic disc containing the nerve fibers to the area of acute vision. For a single eye, this procedure requires up to several hours that are usually divided over a number of treatment sessions.

Although the treatment of this condition by laser photocoagulation was shown to be superior to the other available methods, it suffers from a number of serious problems. The current success rate of this procedure is below 50% for eradication of CNV following one treatment session with a recurrence and/or persistence rate of about 50% [3], [4]. The latter condition requires repeating the treatment. Each treatment repetition in turn has a 50% failure rate. Moreover, several studies indicate that incomplete treatment was associated with poorer prognosis than no treatment [5]. Consequently, the development of an automated laser system to treat the whole retina in one session would significantly impact the outcome of such procedures.

In this paper, we propose a new computerized system for treatment planning and guidance for laser treatment of CNV. This system captures retinal images from a fundus camera and process them to determine the correct positions for laser shots on the retina. Instead of using this time-consuming segmentation procedure repeatedly on the images in the sequence, a fast registration procedure is used to update the positions of a number of landmarks in case of eye movement. The implementation details of the new technique are presented and the results of both the segmentation and registration steps are demonstrated.

II. MATERIALS AND METHODS

A. Data Acquisition System

The retinal images are acquired using a TOPCON TRC-501A fundus camera. This camera has three different operating field of view modes of 50°, 30°, and 15°. All images collected for this paper were acquired using the 50° mode under the red-free illumination mode. A Sony charge coupled device (CCD) video camera was attached to the eyepiece of the fundus camera to make the images collected using the fundus camera available in standard video format. The video output from the CCD camera was connected to a Micron PC (700-MHz Pentium processor, 128 M Bytes of RAM) through a Matrox Meteor video digitizer card. The retinal images were captured to the memory of the computer system either as individual frames or as real-time video sequences. The size of each frame is 640 × 480 pixels of gray-level images. The images were saved on a hard disk for further processing. The images captured in this paper had either normal contrast (darker blood vessels on a bright background) or with the patient injected with the Indocyanine Green dye that gives images with brighter blood vessels relative to a darker background (i.e., reversed contrast).

B. Retinal Image Segmentation Strategy

To determine the validity of a laser shot position, we must be able to identify the locations for sensitive parts of the retina in the acquired images. This is achieved using image segmentation of major vessels in the blood vessel tree, optic disc, and macula to ensure that these areas will not be harmed during laser treatment. Unfortunately, this

task is not straightforward given the complex nature of retinal images [17]. Several studies have been conducted in the area of blood vessel extraction from retinal images as well as from other medical imaging modalities. Generally speaking, these studies can be classified into two main categories: detection of blood vessel boundaries and extraction of the core area of the blood vessel tree by tracing vessel centers.

The first category relies on detecting vessel edges by several techniques. Among those techniques are the use of difference operators and simple thresholding, edge detection based on statistical parameters calculated from the image [9], or edge detection by morphological methods [10], [11]. More recent studies perform contour detection using deformable models [12]–[14]. Edge thresholding techniques are not reliable in detecting small vessels, while detection using image statistics does not perform well under the nonuniform illumination conditions present in retinal images. Moreover, morphological methods often lead to a problem of over-segmentation. On the other hand, detection based on deformable models has been shown to provide more accurate results. Nevertheless, it is not suitable for real-time applications because of its computational complexity and need for user interaction.

In the second category, the goal is to extract the core of blood vessels. It has been noticed that the gray levels across the blood vessel have a Gaussian profile [15]. So, a method to detect the core of the blood vessels by matching the image by two-dimensional (2-D) Gaussian filters was introduced [15]. This algorithm requires a large number of computations when the filter is applied in 12 different directions for best performance. Other techniques using steerable filters have also been used in the detection of the blood vessel core [16], [17]. This class of filters is not applied in many directions. Rather, it is applied in only two basic directions and the response is calculated in other directions from a combination of the responses from these two directions. This has the advantage of faster computation for a reasonable accuracy.

In this paper, we propose an algorithm that extracts the blood vessel tree accurately with a reasonable computational effort in two steps. First, the boundaries of vessels are obtained using a simplified form of deformable models. Then, the core of the wide vessels is determined by correlating the image by a one-dimensional (1-D) Gaussian filter in two perpendicular directions. The proposed methodology combines features from the above two classes of techniques for optimal performance.

C. Detection of Blood Vessel Boundaries Using Deformable Models

In order to detect the boundaries of the blood vessel tree, the initial contour has to grow and converge to the edges of the vessel. The contour growth can be achieved by interpolating the points on the contour using different techniques [12], [14]. Many constraints and user interactions are usually needed, which limit the practicality of this method. In our implementation, the effect of the external energy is made dominant in the energy functional. The image is convolved by a Sobel operator in both the horizontal and vertical directions. The magnitude of the result, which represents the edge values, was taken to represent the external energy of the contour. Instead of selecting a single point having the minimum energy (i.e., maximum edge value) from the neighborhood of each contour point, we search all the neighboring points of each contour point and extract all the points having a value above a certain threshold as new points on the contour. This not only deforms the contour but also makes it grow. Instead of manual initialization of contours, the whole image was covered automatically with an initial set of seed contours [12]. During the contour iteration, the seed contours that lie within the areas of poor edges shrink until vanishing. The others merge and/or split until recovering a continuous description of

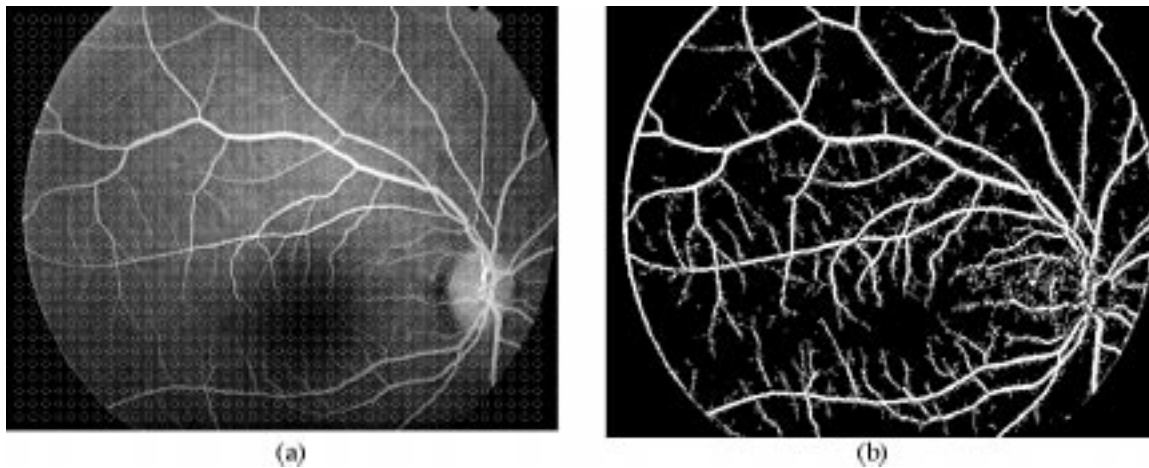


Fig. 1. Example of segmentation results with contrast agent injected. (a) Original image with initial seed contours. (b) Extracted blood vessel tree.

all edges that pass above a certain threshold. This process is repeated until no changes occur during a given iteration. This process leads to the detection of small vessels and only the boundaries of large vessels.

This threshold used in the above procedure changes with every iteration to allow for faster and more accurate convergence. In particular, it is defined as the maximum edge value in the current iteration divided by a parameter that is initialized by the user. All points neighboring a current contour point are compared to this threshold and those having higher values are added as new points on the contour. Since this is applied only for the reference image frame, we are allowed to start with a large value, which we used in this paper as ten. When this process reaches steady-state, this parameter value is divided by a factor of two and the iteration is allowed to run again. This process is repeated until the parameter value reaches a value of one or below. At this point the boundaries of the wide vessel as well as the whole areas of small ones are detected. This iterative refinement optimizes both computational time and accuracy.

D. Core Finding Algorithm

Given that the procedure in [15] provides good results but requires a large number of computations to detect all vessels, we tried to develop a lower complexity form of this procedure. In particular, since small vessels and the boundaries of large vessels have already been detected at an earlier step, we only need to obtain the core of the wide vessels. This is performed by correlating the image with two, 1-D (rather 2-D used in [15]) Gaussian-shaped masks in the vertical and the horizontal directions. The size and form of such masks are selected using the same considerations in [15]. This reduces the computational complexity of the original technique to a great extent and makes it practical for clinical applications. Appendix A1-B shows the mask used in this paper. In order to apply the Gaussian mask to images with reversed contrast, their pixel intensity values are inverted to enable the same mask used for normal contrast to work.

E. Segmenting the Optic Disc

The optic disc is a well-delineated object with properly defined size and edges [24]. In the gray-level retinal images, it always appears as a nearly circular structure that is brighter than the background of the retina. The location of the center point of the optic disc is manually determined to be within a window defined by the user in the reference image. The points inside this window are taken to be possible centers of the optic disc. Then, the Hough transform [24] was applied to detect the center and the radius of optic disc.

F. Segmenting the Macula

The macula appears as a homogeneous area near the optic disc. To segment the macula in the reference frame, the user is asked to point to the fovea (the center of the macula). Then, using a region-growing algorithm, the macula was extracted as the connected region around the fovea having intensities within 20% of the intensity value of the central point. The radius of this region was taken to be double the size of the radius of the optic disc in the y -direction and three times the same radius in the x -direction [24].

G. Estimating the Locations of Laser Shots

After extracting all sensitive objects that must be avoided during laser treatment, a binary image is composed containing these objects. This image was dilated by a flat structuring element of dimensions 7×7 to maintain safety margins around these sensitive areas. The locations of shots are determined by the treating physician on the background areas of the reference image containing no sensitive objects. These locations are updated with every successive image frame [22].

H. Real-Time Movement Tracking

Image registration could be achieved through many ways according to the type of transformation parameters. In [20], a class of algorithms for fast image registration was developed based on similarity detection to evaluate an error function between the mask window and the search image. Among the forms used in this paper is the one employing the difference in the gray levels after normalization (i.e., division by their maximum value). This reduces the number of calculations and gives reasonable results. In [19], an algorithm was presented to obtain the shift by matching and to detect some edge points (using Sobel operator and simple thresholding for example) and their corresponding in the other image, then calculate the angle of rotation between every possible pairs in the two image frames. In this case, if there are n points in the first frame and m points in the second frame, then there are $(n(n-1)/2) \cdot (m(m-1)/2)$ pair to pair comparisons. The angle that has the maximum occurrence is taken to be the global angle of rotation. Even though the technique was successful in some cases, the detected corresponding points include some false points (i.e., incorrect correspondence between points). Moreover, the number of such false points may exceed that of the true points. As a result, the estimated angle may in fact be incorrect in some cases. To solve this problem, an algorithm was presented that detects some landmark points at the vessel branches and crossovers [8]. Then, every pair in the first frame is compared to

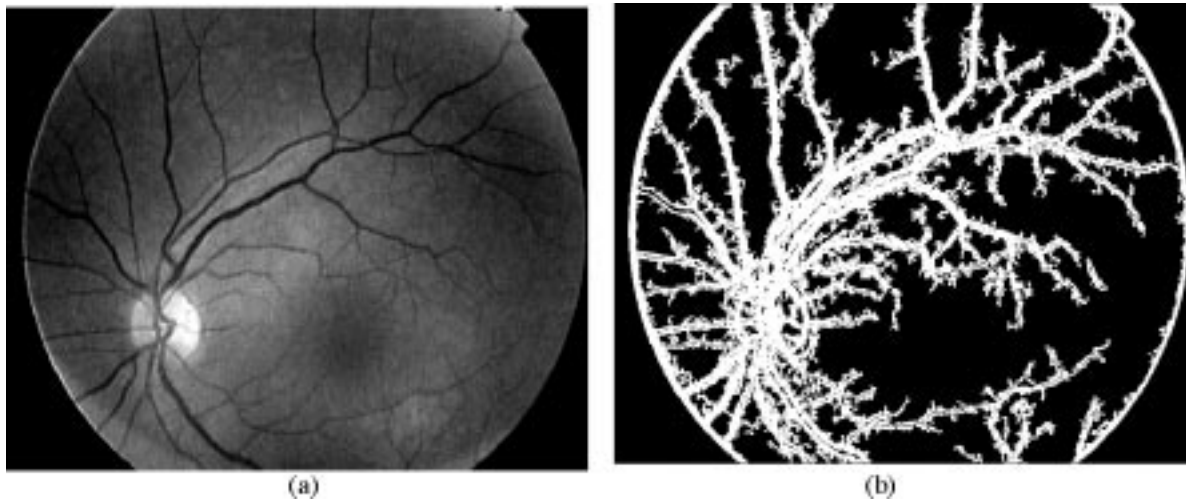


Fig. 2. Example of segmentation results with no contrast agent injected. (a) Original image. (b) Extracted blood vessel tree.

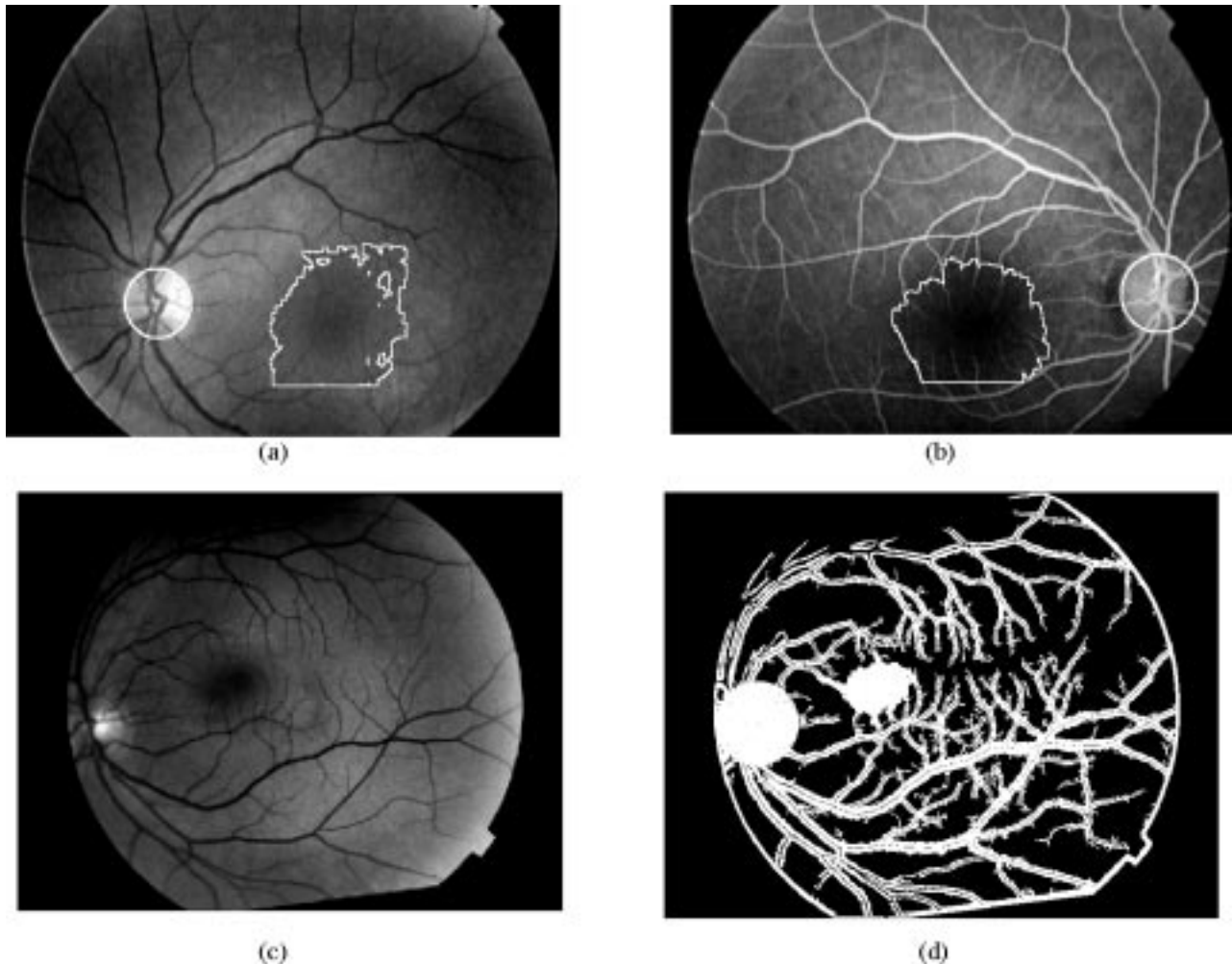


Fig. 3. Demarcation of the optic disc and macula in retinal images (a) without and (b) with contrast agent injected. The final results of segmenting image (c) is shown in image (d) with the macula and optic disc designated as sensitive areas.

every pair in the subsequent frame to extract the pairs that have plausible angles of rotation. Using only these pairs, the scale and shifts are calculated and clustered. Then, the shift and angle of higher occurrence are used to evaluate the transformation through a validation function. This is mainly because some of the estimated landmark points may not have true corresponding points. Even though this technique provides

more accurate results, it requires a large number of computations and thus it is unsuitable for the task of real time retinal tracking.

In this paper, we propose a new fast algorithm to detect corresponding points with lower number of false points. In the retinal images, the points of branching of the large vessels could be taken to be suitable landmark points as defined in [8]. To detect these points,

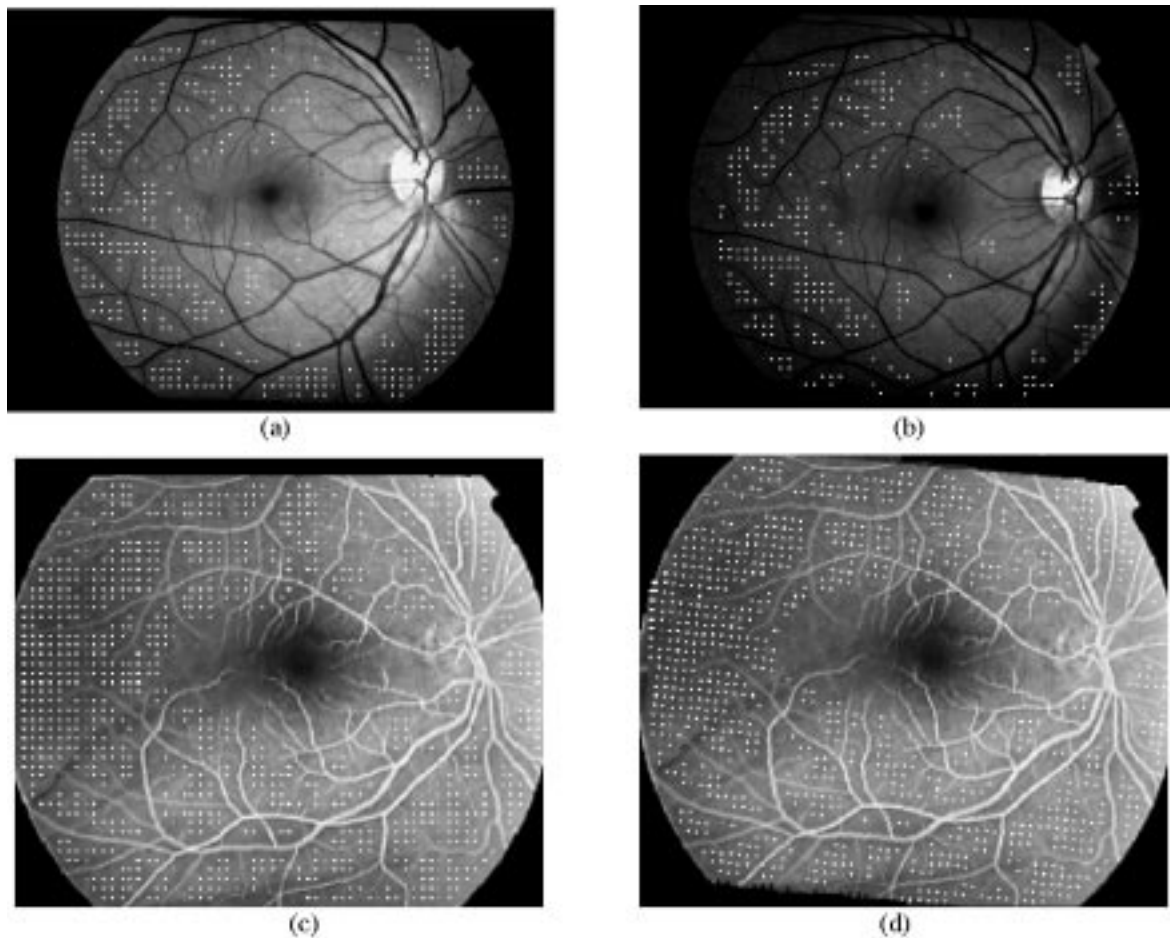


Fig. 4. Illustration of the transformation of laser shot locations between reference and current images. Images (a) and (b) are for images with no contrast agent injected and (c) and (d) are for images with contrast agent injected.

the image is filtered using a 1-D Gaussian mask (similar to the one used for core finding) and thinned using a morphological operator to one pixel thickness. This method extracts the centers of the vessels especially the wide ones and provides a binary image. If we take a window of size 5×5 around the points of branching and crossovers of the wide blood vessels in this binary image, it may have at least five points of ones in this window. So, we search for the points of value one and have at least four points of ones in the 5×5 neighbors, which would be expected to represent the points of branching. If this leads to a number of connected points, the central one is taken as a candidate landmark point. Using this method, we obtain n points in the reference frame and m points in the subsequent frame. We select the optic disc center as the point of origin in the reference frame. By defining a window around the optic disc center and correlating the subsequent frame with this window, we can estimate the corresponding optic disc center, which will also be taken as the point of origin in this image frame. As the retina is assumed to move rigidly (this is true except in case of retinal tears), the points will have the same vector length (magnitudes) relative to each other. So, we compose n pairs of the n points and the point of origin (optic disc center) in the reference frame and m pairs in the subsequent frame. We get the angle of rotation between every one of the n pairs and every one in the m pairs. Then, we have $n \times m$ angles of rotation (note the reduction in the number of calculations). Since the rotation of the retina, if exists, is very close to and does not exceed 5° [8], the pairs that are rotated by angles in the ranges between 4° and 6° as well as those below one degree are extracted. This comparison is made using the absolute value of the

angle since the motion in the opposite direction is possible. The ranges are expanded to compensate for the center of rotation. The magnitudes of the pairs associated with these angles are compared, and those of equal or slightly different magnitudes (half pixel differences) are taken to be corresponding pairs (i.e., corresponding points). This substantially reduces the number of false corresponding points. The points are denoted on the image by small circles. The extracted optic disc center is the center of the solid circle. From these two sets of corresponding points, we can extract the angle of rotation and shift that have the maximum occurrence and compose a transformation vector as $[\text{shift}_x \ \text{shift}_y \ \text{angle}]^T$ to transform the positions of shots estimated in the reference frame to their corresponding locations in the subsequent frame.

Instead of comparing the magnitudes of vectors in the reference and the current frame, we can transform the candidate landmark points in the reference frame to their new position in the current frame using the known Affine transformation matrix composed using the motion parameters. Subtracting the result of this transformation from the corresponding points in the current frame, the point that give a difference less than one half in magnitude are taken as corresponding points.

III. RESULTS AND DISCUSSION

A. Results of Blood Vessel Tree Segmentation

Fig. 1 shows an example of applying the proposed algorithm of segmentation on an Indocyanine Green image, while Fig. 2 illustrates another example of an image with normal contrast. The vessels are accu-

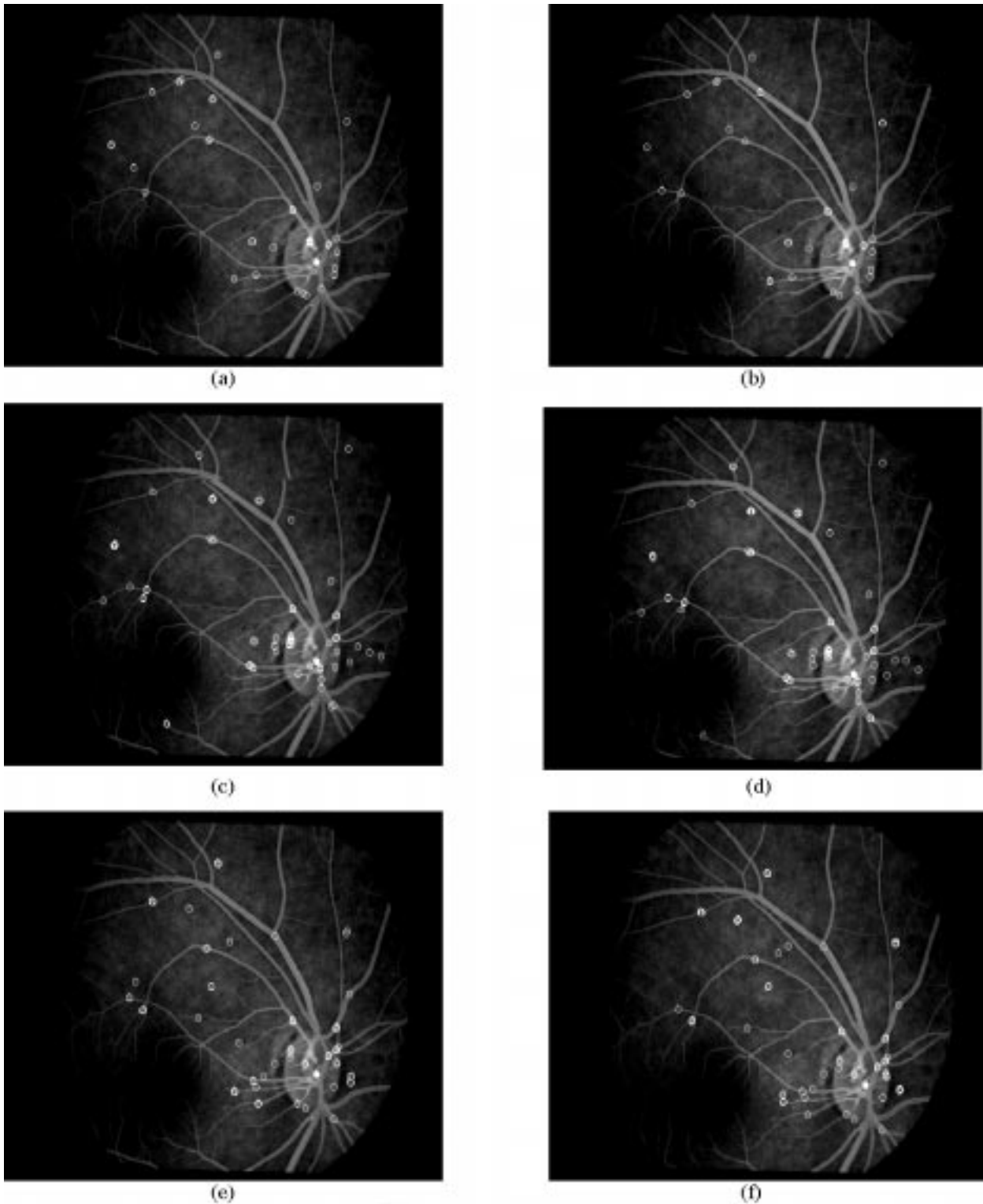


Fig. 5. Examples of landmark tracking showing reference frames and three successive image frames.

rately extracted even when they are small and without sufficient contrast in both cases.

B. Results of Segmenting the Optic Disc and the Macula

Fig. 3(a) and (b) shows the results of extracting the optic disc and demarcating the macula in the above images. The final result of segmentation of Fig. 3(c) is shown in image Fig. 3(d) with both the optic

disc and macula designated as sensitive areas. It can be observed that both structures were accurately delineated.

C. Results of Tracking the Retina and Location Updating

During image capturing, the patient is asked to fixate his eye with respect to the camera in order to get the same scale in all image frames. So, we are only interested in estimating the shift and angle of rotation

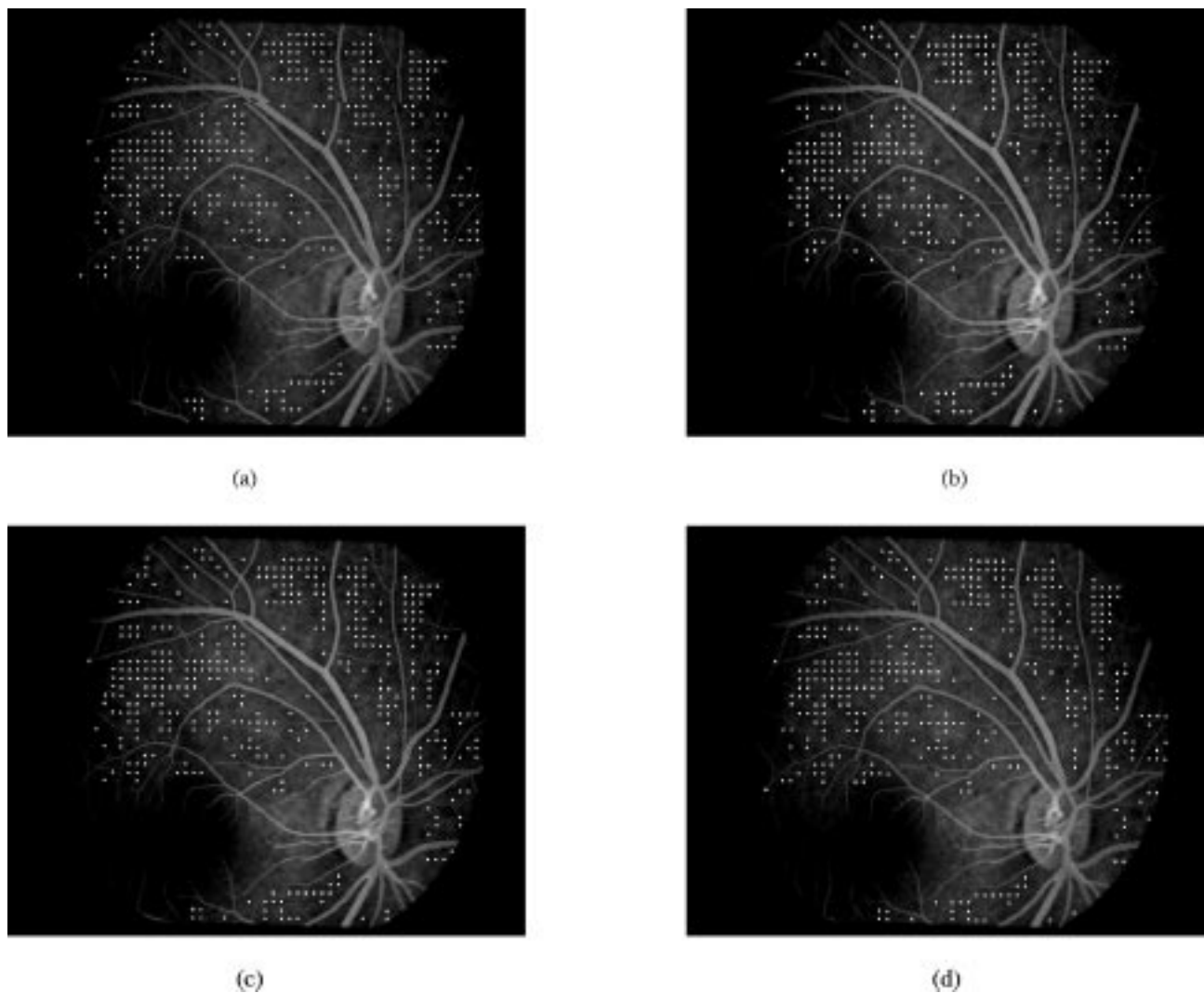


Fig. 6. Laser shot positions on the reference frame and three successive image frames.

between frames. We calculate the shift at the center of gravity of the two landmark points and rotated the estimated positions around it. In this method of tracking, we need to estimate corresponding landmark points. Since we obtain the points of equal or slightly different magnitudes to compensate for the round-off error that may occurs, we may get more than one points in the same neighborhood corresponding to one point. So we take the shift and mean angle of rotation that have the maximum occurrence to compose the transformation vector. In Fig. 4, we present the result of transforming the positions of laser shots to a following frame in an image with normal contrast. Fig. 5 shows the landmark points on the reference frame and their corresponding landmarks in three following frames. As shown in the images in Fig. 5(a) and (b), there are two false corresponding points from a total of 45 corresponding points. In Fig. 5(c) and (d), there is one false point near the optic disc from a total of 86 corresponding landmarks. Fig. 5(e) and (f) shows four false corresponding points from a total of 83 corresponding points. Fig. 6 illustrates the transformation of the estimated locations of laser shots to their new positions in the three subsequent image frames.

Table I shows the results of applying the proposed tracking algorithm on seven image samples with different properties. The simulated shift refers to those cases where we simulated images to include varying degrees of translation and rotation. On the other hand, actual shift refers to shift between actual retinal images in a sequence. The simulated images

were used since all the actual retinal images exhibit translational type of motion only. It was necessary for us to simulated images with rotation to verify this part. In the table, θ is the estimated angle of rotation, C is the estimated center of rotation calculated as the center of gravity of the true landmarks in the subsequent frame, n , m are the numbers of candidate landmarks detected in the reference and subsequent frames respectively, L is the number of corresponding landmarks between the two image frames, *true* is the number of true corresponding landmarks, *false* is the number of false corresponding landmarks, and *time* is the time taken to estimate the transformation vector and updating the locations of laser shots to their new positions. The true corresponding landmarks are only those landmarks having the shifts and rotation of maximum occurrence among the set of corresponding pairs. On the other hand, all other landmarks are considered as false landmarks. The results were computed using a 400-MHz PC to illustrate their practicality for real-time operation. As can be observed, the results seem to provide reasonable computation time even with this modest computational platform. This suggests that significantly faster performance can still be possible by upgrading to a higher speed processing platform.

Future work is needed to resolve some of the limitations not addressed in this paper. An example of that is the case with noncircular optic disc shape. Also, the scaling of images must be fixed throughout the procedure. These limitations can be handled here by using a safety

TABLE I
NUMERICAL RESULTS OF USING THE PROPOSED SYSTEM

Image	x, y shifts (pixel)	θ (deg)	C	n, m	L	True	False	Time (sec)
Simulated shift 640×480 pixels	11,5	5	(331, 222)	247, 307	82	77	5	0.3
Simulated shift 640×480 pixels	5,2	4.5	(293, 297)	350, 309	46	41	5	0.3
Actual shift 640×480 pixels	0,-1	0	(267, 152)	608, 522	57	43	14	0.32
Actual shift 343×296 pixels	43,9	0	(231, 188)	123, 304	4	4	0	0.11
Actual shift 640×480	13,2	0	(381, 198)	331, 203	24	21	3	0.28
Actual shift 640×480	2,11	0	(367, 209)	331, 304	38	37	1	0.3
Actual shift 640×480	-5,14	0	(327, 254)	331, 248	39	38	1	0.31

factor for the radius obtained from the Hough transform procedure and by making sure that the head of the patient is properly fixated and by repeating the acquisition of the reference frame from time to time. Another problem is that the brightness of small areas around laser shot positions increases. This may affect the accuracy of landmark estimation. Some parts of the algorithms can be optimized further. For example, even though the use of Sobel detection in this paper followed the footsteps of [8], the use of other edge detection algorithms such as the Canny edge detector [25] and some of variants [26] should also be investigated.

IV. CONCLUSION

A new computerized system for laser treatment planning was proposed. The new technique performs accurate segmentation on a reference frame and uses fast registration to compute the segmented images of the sequence of images acquired during the treatment. This enables fast tracking of retinal structures and ensures proper administration of the treatment in case of eye movement. The implementation details of the new system are presented and the results demonstrate its clinical value.

APPENDIX

PSEUDOCODE FOR THE ALGORITHMS USED

A. Pseudocode for the Proposed Segmentation Technique

- 1) Generate the seed contour array
- 2) Structuring element = 3×3 array of one's
- 3) Smooth the image
- 4) Get the Gradient Image
- 5) $Th = \max(\text{Gradient image})/\text{threshold}$

- 6) Set NoChanges to false and Final Contour Image array to zeros
- 7) WHILE Threshold > 1 DO
- 8) While NoChanges = FALSE do
- 9) Temporary Contour Image = Contour Image
- 10) Dilate the Contour Image by the Structuring element
- 11) Contour Image = Contour Image AND Image Gradient > Th
- 12) If temporary Contour Image = Contour Image Then NoChanges = TRUE
- 13) End of while
- 14) Gradient Image = zeros where Contour Image = 1
- 15) Final Contour Image = Final Contour Image + Contour Image
- 16) Threshold = Threshold/2
- 17) $Th = \max(\text{Gradient Image})/\text{Threshold}$
- 18) END of WHILE

The average time required for running this algorithm to segment a 640×480 image on a computing platform based on Intel Pentium III 700 processor was about 5 s.

B. Algorithm for Detection of Candidate Landmarks

Start with a reference image R , current image C , a threshold t and the 1-D filter f =

$$\begin{bmatrix} 4 & 3 & 2 & 1 & -2 & -5 & -6 & -5 & -2 & 1 & 2 & 3 & 4 \end{bmatrix}.$$

1- Estimate RefC, the optic disc center using Hough transform.

2- Correlate R with f , take the points above t . The result is RR
 3- Thin RR to one pixel.
 4-Let temp = sum of a 5×5 window over every pixel in RR.
 5- RefLandmarks = points in temp greater than five (points of branching and cross over). If there are some connected points, take the central point. We get n points
 6- Take a window around the optic disc center and get the corresponding center CurrentC in the subsequent frames by matching by correlation coefficient.
 7-Repeat steps from 2-5 for the Current image C to get CurrentLandmarks m points. Then, we have a set of n candidate reference landmarks and a set of m candidate current landmarks.

C. Algorithm to Get the Corresponding Pairs

1- Take RefC as the point of origin and compose m vectors.
 2- Get the slopes of every pair.
 3- Repeat steps 1-2 for CurrentC and get n vectors.
 Every pair in the reference set may have a corresponding pair in the current set. So,
 4- Calculate the angle of rotation for every two pairs $n \times m$ pairs.
 5- Extract the pairs of angles between ± 4 , ± 6 or less than ± 1 .
 6- Compare the magnitudes of the vectors of that range
 7- Obtain the CurrentLandmarks that have vector magnitudes close to those of reference landmarks. Now we have a set of ref points and their corresponding.
 8- Take the angle of rotation and the shifts of maximum occurrence to compose the transformation vector.
 9- Transform the position of laser shots in the reference frame to their corresponding positions in the current frame.

REFERENCES

[1] Macular Degeneration Study Group, "Recurrent choroidal neovascularization after argon laser photocoagulation for neovascular maculopathy," *Arch. Ophthalmol.*, vol. 104, pp. 503-12, 1986.
 [2] S. L. Trokel, "Lasers in ophthalmology," *Opt. Photon. News*, pp. 11-13, Oct. 1992.
 [3] N. M. Bressler, S. B. Bressler, and E. S. Gragoudas, "Clinical characteristics of choroidal neovascular membranes," *Arch. Ophthalmol.*, vol. 105, pp. 209-213, 1987.
 [4] P. N. Monahan, K. A. Gitter, and G. Cohen, "Evaluation of persistence of subretinal neovascular membranes using digitized angiographic analysis," *Retina-J. Retinal, Vitreous Diseases*, vol. 13, no. 3, pp. 196-201, 1993.
 [5] S. Fine, "Observations following laser treatment for choroidal neovascularization," *Arch. Ophthalmol.*, vol. 106, pp. 1524-1525, 1988.

[6] T. M. Clark, W. R. Freeman, and M. H. Goldbaum, "Digital overlay of fluorescein angiograms and fundus images for treatment of subretinal neovascularization," *Retina-J. Retinal Vitreous Diseases*, vol. 2, no. 12, pp. 118-126, 1992.
 [7] L. S. Davis, "A survey of edge detection techniques," *Comput. Graph. Imag. Processing*, vol. 4, pp. 248-270, 1975.
 [8] D. E. Becker, A. Can, J. N. Turner, H. L. Tannenbaum, and B. Roysam, "Image processing algorithms for retinal montage synthesis, mapping, and real-time location determination," *IEEE Trans. Biomed. Eng.*, vol. 45, pp. 105-117, Jan. 1998.
 [9] E. Aniram, H. Aydinoglu, and I. C. Goknar, "Decision based directional edge detector," *Signal Processing*, vol. 35, pp. 149-156, 1993.
 [10] F. Meyer and S. Beuchar, "Morphological segmentation," *J. Vis. Commun. Imag. Representation*, vol. 1, no. 1, pp. 21-46, 1990.
 [11] R. M. Haralick, S. R. Sternberg, and X. Zhuang, "Image analysis using mathematical morphology," *IEEE Trans. Pattern Anal. Machine Intell.*, vol. PAMI-9, pp. 532-550, Apr. 1987.
 [12] T. McInerney and D. Terzopoulos, "Deformable models in medical image analysis: A survey," *Med Image Anal.*, vol. 1, no. 2, pp. 91-108, 1996.
 [13] —, "Topologically adaptable snakes," in *Proc. Int. Conf. Computer Vision (ICCV)*, June 1995, p. 840.
 [14] J. Schnabel, "Active Contours, Snakes, or Deformable Curves," Ph.D. dissertation, Universite Paris-Sud, Paris, France, 1997.
 [15] S. Chaudhuri, C. Chatterjee, N. Katz, M. Nelson, and M. Goldbaum, "Detection of blood vessels in retinal images using two-dimensional matched filters," *IEEE Trans. Med. Imag.*, vol. 8, pp. 263-269, 1989.
 [16] W. T. Freeman and E. H. Adelson, "The design and use of steerable filters," *IEEE Trans. Pattern Anal. Machine Intell.*, vol. 13, pp. 891-906, Sept. 1991.
 [17] B. Kochner, D. Schuhmann, M. Michaelis, G. Mann, and K.-H. Englmeier, "Course tracking and contour extraction of retinal vessels from color fundus photographs: Most efficient use of steerable filters for model based image analysis," in *SPIE Conf. Image Processing*, vol. 3338, 1998, pp. 755-761.
 [18] Q. Zheng and R. Chellappa, "A computational vision approach to image registration," *IEEE Trans. Image Processing*, vol. 2, pp. 311-326, Mar. 1993.
 [19] P. Dani and S. Chandhuri, "Automated assembling of images: Image montage preparation," *Pattern Recogn.*, vol. 28, no. 3, pp. 431-444, 1995.
 [20] D. I. Barnea and H. F. Silverman, "A class of algorithms for fast digital image registration," *IEEE Trans. Comput.*, vol. C-21, pp. 179-186, Feb. 1972.
 [21] B. Peli, R. A. Augliere, and G. T. Timberlake, "Feature-based registration for retinal images," *IEEE Trans. Med. Imag.*, vol. MI-6, pp. 272-278, June 1987.
 [22] S. F. Barrett, M. R. Jerath, H. G. Rylander III, and A. J. Welch, "Digital tracking and control of retinal images," *Opt. Eng.*, vol. 33, no. 1, pp. 150-159, 1994.
 [23] M. S. Markow, H. G. Rylander III, and A. J. Welch, "Real time algorithm for retinal tracking," *IEEE Trans. Biomed. Eng.*, vol. 40, pp. 1269-1281, Dec. 1993.
 [24] A. Pinz, S. Bernogger, P. Datlinger, and A. Kruger, "Mapping the human retina," *IEEE Trans. Med. Imag.*, vol. 17, pp. 606-619, Aug. 1998.
 [25] J. F. Canny, "A computational approach to edge detection," *IEEE Trans. Pattern Anal. Machine Intell.*, vol. PAMI-8, pp. 679-698, Nov. 1986.
 [26] R. Deriche, "Using Canny's criteria to derive a recursively implemented optimal edge detector," *Int. J. Comput. Vis.*, vol. 1, no. 2, pp. 167-187, May 1987.